Author(s): Hannula, Jari-Matti & Rasilainen, Kimmo & Viikari, Ville

Title: Characterization of Transponder Antennas Using Intermodulation Response

Year: 2015

Version: Post print

Please cite the original version:

Hannula, Jari-Matti & Rasilainen, Kimmo & Viikari, Ville. 2015. Characterization of Transponder Antennas Using Intermodulation Response. IEEE Transactions on Antennas and Propagation. Volume 63, Issue 6. 2412-2420. DOI: 10.1109/tap.2015.2414438.

Characterization of Transponder Antennas Using Intermodulation Response

Jari-Matti Hannula, Kimmo Rasilainen, and Ville Viikari, *Senior Member, IEEE*

***Abstract*—The intermodulation measurement technique enables measuring transponder antennas without any cable connections. This contactless technique exploits the inherent nonlinearity of the transponder to generate intermodulation products that can be measured. In this paper, we relate the transponder antenna properties to the intermodulation response, and use this relation to calculate the gain and impedance matching of the transponder antenna. Additionally, we consider the limitations of the measurement method and present three different measurement geometries for measuring the radiation pattern. The presented equations and methods are experimentally verified by measuring an example harmonic transponder.**

***Index Terms*—Antenna measurements, harmonic radar, intermodulation distortion, mixers, radiofrequency identification (RFID), transponders, wireless sensors.**

I. Introduction

TRANSPONDERS incorporating nonlinear components are used, e.g., in radiofrequency identification (RFID), harmonic transponders [1], intermodulation sensors [2]–[6] and other passive wireless sensors [7]. The nonlinearity in the transponder is used for rectification, for harmonic generation, and for modulation. RFID transponders rectify DC voltage from the received RF signal to operate their logic circuits. The rectifier is also used as a modulator in the modulated backscattering principle of RFID. Harmonic transponders and intermodulation sensors, on the contrary, utilize the nonlinearity for producing harmonic and intermodulation frequencies.

Experimental characterization of transponder antennas can be challenging. They are typically matched to a chip or diode, whose impedance is complex and can be far from the traditional 50-Ω level, which can be inherently difficult for conventional measurement equipment. Studies on such antennas can be found, e.g., in [8]. In addition, conventional techniques require a cable connection to the antenna. Transponders operate without cables, so connecting a cable may be difficult. A cable connection can easily change the radiation properties of an antenna, in particular when the antenna is electrically small. The cable may additionally require a balun and possibly an adapter, further complicating the testing.

Harmonic transponders have been used, e.g., for tracking insects [9]–[11] and locating avalanche victims [12]. These transponders, when illuminated at one fundamental frequency f_0, scatter back at the second harmonic frequency $2f_0$. Measurement of these transponders is a particular challenge, because the harmonic response of the transponder depends on the antenna gain and matching at both the fundamental and the second harmonic frequencies [13]. Therefore, it is impossible to find out how well the antenna is matched at one frequency and what is the radiation pattern at that frequency if only the harmonic response is measured. As a consequence, this limited information does not facilitate diagnosis of the transponder operation nor improvement of it.

One way to overcome the challenges related to cables is to use contactless measurement techniques [14], [15]. In these techniques, the scattered signal from an antenna is measured by connecting different known loads at the antenna port. Such methods have been developed for antenna gain [16] and impedance [17], [18]. Although a cable is not needed, the methods necessitate that the antenna port can be terminated with different known loads. This may be problematic, for instance if the antenna is integrated with an RF front-end.

The radiation pattern of a transponder antenna can also be measured by illuminating the transponder by a reader device and recording the transponder response as a function of its rotation angle. These kind of automated systems are commercially available for RFID [19], but the same is difficult to do with conventional laboratory equipment, because standard devices cannot properly emulate an RFID reader.

Another contactless measurement method is the intermodulation measurement technique, which was used to measure the radiation pattern of a UHF RFID transponder in [20]. In this technique, the transponder is illuminated with two closely located frequencies f_1 and f_2. Due to the inherent nonlinearity in the transponder, it scatters back a signal containing intermodulation frequencies $nf_1 \pm mf_2$ of the excitation signal (n and m are integers). In [20], the idea of the method is shortly described and the method is experimentally demonstrated without detailed analysis or considerations.

In this paper, we expand the intermodulation measurement technique in many ways. First, we relate the antenna properties to the intermodulation response of the transponder. This relation is needed for solving the antenna properties from the measured response. Further, we describe different measurement geometries and show how the measurement geometry affects the dynamic range and radiation pattern calculation. Monostatic, bistatic and multistatic geometries are studied. In addition to the antenna pattern, matching between the antenna and the circuitry (diode or RFID chip) is important. We show how the impedance matching can be obtained from the measured intermodulation response of the transponder.

The dynamic range in the intermodulation measurement

Manuscript submitted December 17, 2014; revised February 19, 2015; accepted March 14, 2015. This work was supported in part by the Academy of Finland under the decision 267420, by Aalto ELEC Doctoral School and by the Nokia Foundation.

The authors are with the Department of Radio Science and Engineering, Aalto University School of Electrical Engineering, Otakaari 5A, P.O. Box 13000, FI-00076, AALTO, Finland (e-mail: jari-matti.hannula@aalto.fi).

This article has been accepted for publication in a future issue of this journal, but has not been fully edited. Content may change prior to final publication. Citation information: DOI 10.1109/TAP.2015.2414438, IEEE Transactions on Antennas and Propagation

technique is typically limited by the intermodulation distortion of the measurement equipment itself. In this paper, we derive equations for the dynamic range of the measurement principle. These equations are needed for proper design of the measurement system.

As the transponders are inherently nonlinear, their operation also changes with input power. This is problematic, e.g., for measuring the radiation pattern. When the transponder is rotated, the power it receives changes due to a different antenna gain towards the reader. Then, it is difficult to find out how much the backscattered signal changed due to change in the directivity, and how much due to change in the excitation power. In this paper, we describe how this problem can be avoided.

The explained measurement principle is superior over any other way for characterizing harmonic transponders, but can also be beneficial for measuring other than transponder antennas, especially in cases where a cable connection to the antenna must be avoided.

II. Intermodulation Response

In this section, we relate the antenna properties to the intermodulation response of the transponder (tag). Using the derived relation, we further show how the antenna properties are obtained from the measured response. We also consider the limitations of the model and how they affect the dynamic range of the measurement method.

A. Analytical Response

The intermodulation response of a transponder is measured by illuminating it with two closely located frequencies f_1 and f_2. These two frequencies are mixed, generating intermodulation products at several frequencies, including $2f_1 - f_2$ and $2f_2 - f_1$. Backscattered signal at one of these frequencies is recorded. Because all three frequencies are closely located, the intermodulation response can be approximated to depend on the antenna properties at only one frequency.

The power transmitted to the transponder at one frequency can be obtained from the Friis transmission equation

$$P_{\mathrm{in}} = P_{\mathrm{t}} G_{\mathrm{t}} G_{\mathrm{tag}} \left(\frac{\lambda}{4\pi r_{\mathrm{t}}} \right)^2 \tag{1}$$

where P_{in} is the power received by the transponder and P_{t} is the transmitter input power. The gain of the transmitter $G_{\mathrm{t}} = G_{\mathrm{tc}} G_{\mathrm{ta}}$ consists of the gain of the transmitter chain (amplifiers, cables, etc.) G_{tc} and that of the transmitter antenna G_{ta}. G_{tag} is the gain of the transponder antenna, λ is the wavelength and r_{t} is the distance between the transmitter and the transponder. The offset $f_2 - f_1$ is assumed to be small, such that $f_1 \approx f_2$ and the transmitted power is equal at both frequencies.

Next, the output power of the transponder at the intermodulation frequency is calculated. We model the transponder with the electrical equivalent circuit shown in Fig. 1. Without a loss of generality, the antenna and possible matching circuit are modelled as a generator with an internal resistance of R_{a} and reactance of X_{a}, both of which may depend on the frequency. To facilitate the experiments in the paper, the nonlinear component in the transponder is assumed to be a Schottky diode, which is modeled as a series inductance L_{s}, a parasitic capacitance C_{p}, a series resistance R_{s}, a small-signal junction resistance R_{j}, and a small-signal junction capacitance C_{j0}. Modifications of the following equations for other nonlinear elements can be considered straightforward.

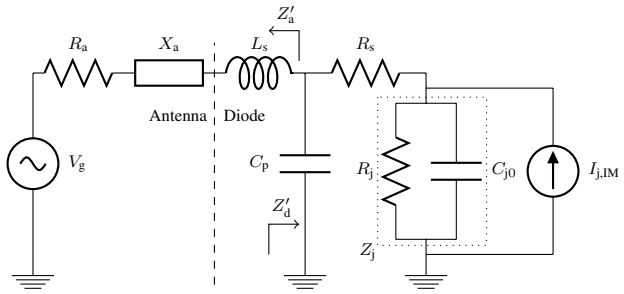

Fig. 1. Small-signal circuit model for a harmonic transponder.

The voltage generated by the antenna is

$$V_{\mathrm{g}} = 2\sqrt{2R_{\mathrm{a}}P_{\mathrm{in}}}(\sin(\omega_1 t) + \sin(\omega_2 t)). \tag{2}$$

The corresponding voltage across the junction of the Schottky diode is

$$V_{\mathrm{j}} = \frac{Z_{\mathrm{j}}}{R_{\mathrm{s}} + Z_{\mathrm{j}}} \frac{Z'_{\mathrm{d}}}{Z'_{\mathrm{a}} + Z'_{\mathrm{d}}} V_{\mathrm{g}} \tag{3}$$

where $Z'_{\mathrm{d}} = \left(\jmath\omega C_{\mathrm{p}} + (R_{\mathrm{s}} + Z_{\mathrm{j}})^{-1}\right)^{-1}$, $Z'_{\mathrm{a}} = R_{\mathrm{a}} + \jmath X_{\mathrm{a}} + \jmath\omega L_{\mathrm{s}}$ and $Z_{\mathrm{j}} = (1/R_{\mathrm{j}} + \jmath\omega C_{\mathrm{j0}})^{-1}$. The series inductance is included in the antenna impedance Z'_{a} to simplify the analysis. This voltage generates a current in the diode, and the junction current is [13]

$$I_{\mathrm{j}}(V_{\mathrm{j}}) = I_{\mathrm{s}}(e^{\alpha V_{\mathrm{j}}} - 1) + \frac{\mathrm{d}}{\mathrm{d}t}\left\{ \frac{\Phi C_{\mathrm{j0}}}{1-\gamma} \left(1 - \frac{V_{\mathrm{j}}}{\Phi}\right)^{-\gamma+1} \right\} \tag{4}$$

where I_{s} is the saturation current, $\alpha = q/nkT$ where q is the elementary charge, n is an ideality factor, k is the Boltzmann constant and T is the temperature, Φ is the junction potential, C_{j0} is the junction capacitance under zero bias, and γ is a profile parameter. The resulting current can be represented as a current source parallel to the junction, as seen in Fig. 1. The third order Taylor approximation for the junction current is

$$\begin{aligned} I_{\mathrm{j}}(V_{\mathrm{j}}) \approx & \frac{V_{\mathrm{j}}}{R_{\mathrm{j}}} + C_{\mathrm{j0}} \frac{\mathrm{d}}{\mathrm{d}t}\{V_{\mathrm{j}}\} + \frac{\alpha V_{\mathrm{j}}^2}{2R_{\mathrm{j}}} + \frac{C_{\mathrm{j0}}\gamma}{2\Phi} \frac{\mathrm{d}}{\mathrm{d}t}\{V_{\mathrm{j}}^2\} \\ & + \frac{\alpha^2}{6R_{\mathrm{j}}} V_{\mathrm{j}}^3 + \frac{C_{\mathrm{j0}}\gamma(\gamma+1)}{6\Phi^2} \frac{\mathrm{d}}{\mathrm{d}t}\{V_{\mathrm{j}}^3\} \end{aligned} \tag{5}$$

where $R_{\mathrm{j}} = 1/\alpha I_{\mathrm{s}}$. The first and second order terms can be ignored as only the third-order terms contribute to the intermodulation response. For an excitation signal at angular frequencies ω_1 and ω_2 with amplitude $\hat{V}_{\mathrm{j}}$, the relevant third order intermodulation frequencies are

$$\begin{aligned} & (\hat{V}_{\mathrm{j}}(\sin(\omega_1 t) + \sin(\omega_2 t)))^3 = \\ & \frac{3}{4}\hat{V}_{\mathrm{j}}^3(\sin((2\omega_1 - \omega_2)t) + \sin((2\omega_2 - \omega_1)t)) + \ldots) \end{aligned} \tag{6}$$

either of which can be selected to be measured. For convenience, the selected intermodulation frequency is subsequently

This article has been accepted for publication in a future issue of this journal, but has not been fully edited. Content may change prior to final publication. Citation information: DOI 10.1109/TAP.2015.2414438, IEEE Transactions on Antennas and Propagation

referred to as f_{IM}. The junction current at the intermodulation frequency $I_{\mathrm{j,IM}}$ can be solved by substituting (2), (3), and (6) into (5). Using current division, the current through the antenna $I_{\mathrm{a,IM}}$ can be calculated, which can then be used to solve the radiated output power

$$P_{\mathrm{out,IM}} = \frac{1}{2}R_{\mathrm{a}}|I_{\mathrm{a,IM}}|^2 = 4\left|\frac{\alpha^2}{R_{\mathrm{j}}} - \jmath\frac{\omega C_{\mathrm{j0}}\gamma(\gamma+1)}{\Phi^2}\right|^2\left|\frac{Z_{\mathrm{j}}}{R_{\mathrm{s}}+Z_{\mathrm{j}}}\right|^8\left|\frac{Z'_{\mathrm{d}}}{Z'_{\mathrm{a}}+Z'_{\mathrm{d}}}\right|^8 R_{\mathrm{a}}^4 P_{\mathrm{in}}^3. \tag{7}$$

Here, it is assumed that $f_1 \approx f_2 \approx f_{\mathrm{IM}}$ and that all frequency-dependent variables are equal at these frequencies.

To facilitate solving the matching between the antenna and the diode, we relate the impedances of the antenna and the diode to the reflection coefficient with the following notation

$$\frac{4R_{\mathrm{a}}R_{\mathrm{d}}}{|Z'_{\mathrm{a}}+Z'_{\mathrm{d}}|^2} = 1-|S_{11}|^2 \tag{8}$$

where R_{d} is the resistance of the diode and S_{11} is the reflection coefficient between the antenna and the diode [21]. By substituting (8) into (7) the output power becomes

$$\begin{aligned} P_{\mathrm{out,IM}} =& \frac{1}{64R_{\mathrm{d}}^4}\left|\frac{\alpha^2}{R_{\mathrm{j}}} - \jmath\frac{\omega C_{\mathrm{j0}}\gamma(\gamma+1)}{\Phi^2}\right|^2\left|\frac{Z_{\mathrm{j}}}{R_{\mathrm{s}}+Z_{\mathrm{j}}}Z'_{\mathrm{d}}\right|^8 \\ &\cdot(1-|S_{11}|^2)^4 P_{\mathrm{in}}^3 \\ =& E_{\mathrm{IM}}(1-|S_{11}|^2)^4 P_{\mathrm{in}}^3 \end{aligned} \tag{9}$$

where we denote the intermodulation properties of the load with E_{IM}. The intermodulation product at the receiver can then be solved by using the Friis transmission equation twice. The response at the receiver becomes

$$P_{\mathrm{r,IM}} = \underbrace{P_{\mathrm{t}}^3\frac{G_{\mathrm{t}}^3 G_{\mathrm{r}}}{r_{\mathrm{t}}^6 r_{\mathrm{r}}^2}\left(\frac{\lambda}{4\pi}\right)^8}_{\text{setup}}\underbrace{G_{\mathrm{tag}}^4(1-|S_{11}|^2)^4}_{\text{realized gain of antenna}}\underbrace{E_{\mathrm{IM}}}_{\substack{\text{mixing}\\ \text{element}}} \tag{10}$$

where G_{r} is the gain of the receiver antenna and r_{r} is the distance between the transponder and the receiver. This form separates the three factors affecting the intermodulation response: measurement setup, antenna properties, and mixing element properties. It is also valid for different transponder types, the only difference being the value of E_{IM}.

B. Dependency on Input Power

It is assumed in (10) that the transponder operates under small-signal conditions. This assumption is only valid when the power received by the transponder is small. At higher power levels, the junction resistance R_{j} of the diode changes due to self-biasing. Also, the small-signal approximation is less accurate when the AC voltage swing is large. The power delivered to the transponder should therefore be kept constant to ensure that the transponder is operating under small-signal conditions during the whole measurement. This can be done by selecting a reference frequency f_{ref} and input power $P_{\mathrm{t,ref}}$ at which the model is valid. Changes in frequency, gain and matching can then be compensated by adjusting the input power to

$$P_{\mathrm{t,adj}} = P_{\mathrm{t,ref}}\frac{G_{\mathrm{tag,ref}}(1-|S_{11,\mathrm{ref}}|^2)}{G_{\mathrm{tag}}(1-|S_{11}|^2)}\left(\frac{f}{f_{\mathrm{ref}}}\right)^2 \tag{11}$$

where $P_{\mathrm{t,adj}}$ is the adjusted input power and $G_{\mathrm{tag,ref}}$ and $S_{11,\mathrm{ref}}$ are the gain and reflection coefficient at the reference frequency. In a radiation pattern measurement only the gain value changes, which simplifies the expression. Initial impedance matching or radiation pattern calculations can be done using constant input power, and the input power can be adjusted in the next measurement based on these initial results. This process can be repeated, iterating multiple times until the calculated values remain constant between iterations.

C. Dynamic Range

The dynamic range of the measurement can be limited by four factors: input power, noise, transponder nonlinearity and intermodulation distortion from the measurement equipment itself. Ideally, the response from the transponder should be stronger than the interference at all times. However, at some frequencies or rotational angles the response can be obscured by the distortion generated by the transmitter or the receiver. Theoretically, both the measured response from the tag and the intermodulation distortion of the measurement equipment depend in the same way on the excitation power. Therefore the dynamic range cannot be improved by increasing the transmit power in cases where the lowest detectable signal is limited by intermodulation distortion rather than noise.

The distortion in the transmitter can be caused by the signal generators or the amplifiers as they are not completely isolated from their counterparts, i.e. the signal at f_1 leaks to the instrument generating f_2. This coupling results in mixing occurring in the devices, which then generates intermodulation distortion that is transmitted. The distortion in the receiver is caused by the two input signals directly coupling to the receiver and generating intermodulation products in the spectrum analyzer. The total received noise and interference power at the intermodulation frequency is

$$P_{\mathrm{NI}} = P_{\mathrm{N}} + \frac{|S_{21}|^2 P_{\mathrm{t}}^3}{LOIP_{3,\mathrm{t}}^2} + \frac{(P_{\mathrm{t}}|S_{21}|^2)^3}{L^3 OIP_{3,\mathrm{r}}^2} \tag{12}$$

where P_{N} is the noise power, L is attenuation before the receiver, $|S_{21}|^2$ the coupling between the transmitter and receiver, and $OIP_{3,\mathrm{t}}$ and $OIP_{3,\mathrm{r}}$ are the third order intercept points of the transmitter and the receiver.

The coupling between the transmitter and receiver antennas should be minimized first, as it decreases distortion caused by both the transmitter and receiver. The distortion in the transmitter can be reduced by increasing the isolation between the two signal generators to limit the mixing that occurs in them. The isolation should be made as high as possible with the available equipment as it does not reduce the dynamic range of the system. In the receiver, the distortion can be reduced by attenuating the received signal. Eq. (12) indicates that the interference power is inversely proportional to the third power of attenuation. Because the signal attenuates in

This article has been accepted for publication in a future issue of this journal, but has not been fully edited. Content may change prior to final publication. Citation information: DOI 10.1109/TAP.2015.2414438, IEEE Transactions on Antennas and Propagation

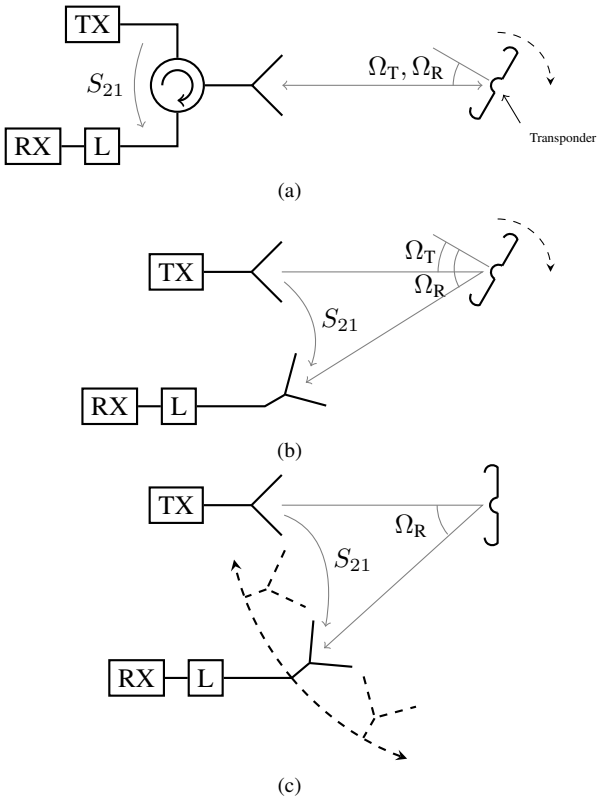

Fig. 2. Three radiation pattern measurement geometries. (a) Monostatic (b) Bistatic (c) Multistatic. TX refers to the transmitter system and RX to the receiver. L is the attenuation before the receiver.

the first power of L, it is advantageous to adjust L so that the interference is at the same level as noise. This maximizes the dynamic range.

The optimal amount of attenuation can be calculated. To do so, let us define the signal-to-interference-plus-noise-ratio (SINR) for the system as

$$\mathrm{SINR} = \frac{P_{\mathrm{r,IM}}/L}{P_\mathrm{N} + \frac{|S_{21}|^2 P_\mathrm{t}^3}{LOIP_{3,\mathrm{t}}^2} + \frac{(P_\mathrm{t}|S_{21}|^2)^3}{L^3 OIP_{3,\mathrm{r}}^2}}. \tag{13}$$

The optimal attenuation is found by solving the maximum of SINR as a function of L. Differentiating the equation and solving the zero gives the optimal attenuation as

$$L = P_\mathrm{t}|S_{21}|^2 \sqrt[3]{\frac{2}{P_\mathrm{N} OIP_{3,\mathrm{r}}^2}}. \tag{14}$$

On the other hand, the dynamic range also has an upper limit. As was mentioned earlier, if the input power is increased too much, the nonlinearity of the transponder becomes a problem. This limits the maximum usable input power. The input power can also be limited because of the measurement equipment used.

III. Radiation Pattern Measurement Geometries

The gain of the antenna can be solved from (10). Note that the intermodulation response depends both on the reflection coefficient $|S_{11}|$ and the gain of the antenna G_tag. Both of these cannot be solved simultaneously from the response only. If the reflection coefficient is not known, one can solve the realized gain

$$G_{\mathrm{R,tag}} = (1 - |S_{11}|^2) G_\mathrm{tag} \tag{15}$$

instead, which combines both unknowns. The gain depends on the orientation of the transponder, so we denote the realized gain $G_{\mathrm{R,tag}}$ with $G(\theta, \phi) = G(\Omega)$, where Ω is the orientation angle of the transponder, consisting of θ and ϕ, the polar and azimuthal angles in spherical coordinates.

The response is proportional to $G(\Omega_\mathrm{T})^3 G(\Omega_\mathrm{R})$, where the subscripts T and R refer to the angular orientation of the transponder with respect to the transmitter and the receiver. The realized gain as a function of intermodulation response is

$$\begin{aligned} G(\Omega_\mathrm{T})^3 G(\Omega_\mathrm{R}) &= \left(\frac{4\pi}{\lambda}\right)^8 \frac{r_\mathrm{t}^6 r_\mathrm{r}^2}{G_\mathrm{t}^3 G_\mathrm{r} E_\mathrm{IM} P_\mathrm{t}^3} P_{\mathrm{r,IM}} \\ &= A P_{\mathrm{r,IM}} \end{aligned} \tag{16}$$

where all angle-independent terms in the equation are combined to A to shorten subsequent equations. Gain pattern can be obtained if A can be evaluated precisely. Otherwise only a relative radiation pattern can be obtained. This paper presents three different configurations for measuring the radiation patterns, as illustrated in Fig. 2.

A. Monostatic Measurement

If one antenna is used to both transmit and receive, then $\Omega_\mathrm{R} = \Omega_\mathrm{T}$ and the gain can be solved directly from (16). The gain is

$$G(\Omega_\mathrm{T}) = \sqrt[4]{A P_{\mathrm{r,IM}}(\Omega_\mathrm{T})} \tag{17}$$

where Ω_T is the rotation angle of the transponder and $P_{\mathrm{r,IM}}(\Omega_\mathrm{T})$ the measured response when the transponder is oriented to direction Ω_T. The advantage of this method is that it requires only one antenna and the calculation of the gain is simple. The dynamic range of the method can be poor as the coupling from the transmitter to the receiver can be relatively strong, potentially resulting in significant interference. The response can also be too weak to be distinguished from the noise when a radiation pattern minimum is aligned towards the transceiver antenna as the response is proportional to G^4.

B. Bistatic Measurement

Bistatic measurement is similar to the previous case, except that the transmitter and receiver are using separate antennas at different locations. In the measurement, both antennas remain stationary while the transponder is rotated. The measured power as a function of transponder gain is therefore

$$G(\Omega_\mathrm{T})^3 G(\Omega_\mathrm{T} + \Omega_\Delta) = A P_\mathrm{r}(\Omega_\mathrm{T}). \tag{18}$$

where Ω_Δ is the offset between the transmitter and the receiver on the rotation plane. The offset should be equal to or a multiple of the angular step in the measurement. The method necessitates that the measurement angles are evenly distributed over a full circle. By denoting the measurement points with $G_1, \ldots, G_n$, equation (18) can then be modified to

$$3G_i + G_{i+\Delta} = A + P_{\mathrm{r},i} \tag{19}$$

This article has been accepted for publication in a future issue of this journal, but has not been fully edited. Content may change prior to final publication. Citation information: DOI 10.1109/TAP.2015.2414438, IEEE Transactions on Antennas and Propagation

where all quantities are in decibels and Δ is the offset of the antennas in angular steps. The indices are cyclic, so that, e.g., $G_{n+1} = G_1$. A matrix equation can be formed from all the measured values and the measured gain can be solved by inverting the coefficient matrix and multiplying both sides of the equation by the inverse matrix. The gain is

$$\begin{pmatrix} G_1 \\ G_2 \\ \vdots \\ G_{n-1} \\ G_n \end{pmatrix} = \begin{pmatrix} 3 & \cdots & 1 & \cdots & 0 \\ 0 & 3 & \cdots & 1 & \vdots \\ \ddots & \ddots & \ddots & \ddots & \ddots \\ \vdots & 1 & \ddots & 3 & 0 \\ 0 & \cdots & 1 & \cdots & 3 \end{pmatrix}^{-1} \begin{pmatrix} A + P_{\mathrm{r},1} \\ A + P_{\mathrm{r},2} \\ \vdots \\ A + P_{\mathrm{r,n}-1} \\ A + P_{\mathrm{r,n}} \end{pmatrix}. \tag{20}$$

Generally speaking, the offset between the antennas can be chosen freely. However, the choice of the offset can be used to optimize the dynamic range of the measurement. The offset can be selected to minimize the coupling between the transmitter and the receiver, decreasing the distortion generated. Alternatively, the offset can be selected based on the radiation pattern. Depending on the radiation pattern of the transponder, it might be possible to have one antenna aligned towards the maximum when the other is aligned towards a minimum (possible for, e.g., a dipole) so that the response is only G^3 smaller than the highest response (as opposed to the monostatic case where it is G^4 smaller). In this method, the response depends on the gain at two different positions, which complicates the gain calculation. The gain can also be measured only in one plane at a time. Additionally, a limited dynamic range can also cause inaccuracies in the pattern even outside the minima.

C. Multistatic measurement

In multistatic geometry, the intermodulation response is measured using multiple receiver antenna locations. In practice, the measurement is done by moving the receiver antenna around the static transponder and recording the response at each location. When only the receiver antenna is moved, the relative gain can be solved as a function of Ω_{R}

$$G(\Omega_{\mathrm{R}}) = AP_{\mathrm{r}}(\Omega_{\mathrm{R}})/G(\Omega_{\mathrm{T}})^3. \tag{21}$$

As the transmitter and the transponder are static with respect to each other, $G(\Omega_{\mathrm{T}})^3$ is constant. Thus the normalized pattern is obtained directly from P_{r}. In order to solve the maximum gain, one measurement point should be such that $\Omega_{\mathrm{T}} = \Omega_{\mathrm{R}}$ in which case (17) can be used.

This is equivalent to rotating both the transmitter antenna and the transponder while keeping the receiver antenna stationary, as was done in [20]. This method has the advantage of illuminating the transponder with constant input power at all angles, so there is no need for power level adjustment. The transmitter can be positioned towards a maximum in the pattern to maximize the response. The response is directly proportional to the transponder gain so it should theoretically provide the best dynamic range. This option requires either integrating the transmitter antenna to the turntable with the transponder or the ability to move the receiver antenna along a circle. These can be more complicated to build as compared to rotating only the measured transponder.

IV. Resonance Frequencies and Impedance Matching

The magnitude of the received intermodulation response depends on the impedance matching between the antenna and the nonlinear mixing element. The resonance frequencies of the antenna appear as local maxima in the intermodulation response.

The transponder antenna impedance can be fully solved from complex (amplitude and phase) intermodulation response. The laboratory equipment available for the following experiments, however, facilitates only amplitude measurements. Due to this limitation, we can only solve the absolute value of the reflection coefficient between the antenna and the non-linear element. Solving $|S_{11}|^2$ from (10) gives

$$|S_{11}|^2 = 1 - \sqrt[4]{\frac{r_{\mathrm{t}}^6 r_{\mathrm{r}}^2}{G_{\mathrm{tag}}^4 G_{\mathrm{t}}^3 G_{\mathrm{r}} E_{\mathrm{IM}}} \frac{P_{\mathrm{r,IM}}}{P_{\mathrm{t}}^3}} \left(\frac{4\pi}{\lambda}\right)^2. \tag{22}$$

This assumes that the gain of the transponder G_{tag} is known at all measured frequencies. One option is to estimate the gain using simulations. Alternatively, one could instead solve the realized gain from (16) as a function of frequency.

The offset between the transmitted and intermodulation frequencies should be made reasonably small. If the offset is too large, there will be some error in the results due to averaging. This is especially notable in the case of narrowband matching as the matching level can be significantly different at each of the frequencies.

Although the technique cannot be used to obtain the impedance directly, obtaining information about the matching can be quite useful in designing and improving transponder antennas. The method shows clearly if the resonance frequencies have shifted from the designed values and obtains the bandwidth. These values are relatively reliable in the sense that they are obtained by terminating the antenna with its real load. The measurement can also be performed when the transponder is attached to an object, as was done in [20]. Further information about the antenna impedance may be obtained by fitting an equivalent circuit model to the measured reflection coefficient.

V. Experiments

The techniques described above are verified using a prototype harmonic transponder with resonance frequencies at 1 and 2 GHz. The transponder itself has been analyzed in [13]. The diode in the transponder is an SMV2019 varactor diode, manufactured by Skyworks Solutions Inc. [22]. The diode parameters used in the calculations and simulations are obtained from the SPICE model provided by the manufacturer.

A. Measurement Setup

The measurement is performed using a configuration similar to the one in [20]. The input signals are generated with two signal generators, Rohde & Schwarz SML-03 and SMT-06.

This article has been accepted for publication in a future issue of this journal, but has not been fully edited. Content may change prior to final publication. Citation information: DOI 10.1109/TAP.2015.2414438, IEEE Transactions on Antennas and Propagation

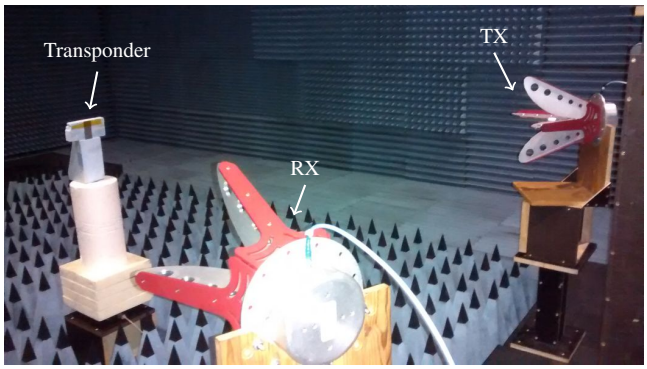

Fig. 3. Bistatic measurement setup in the anechoic chamber, showing transmitting and receiving ridged-horn antennas, and the transponder on a turntable.

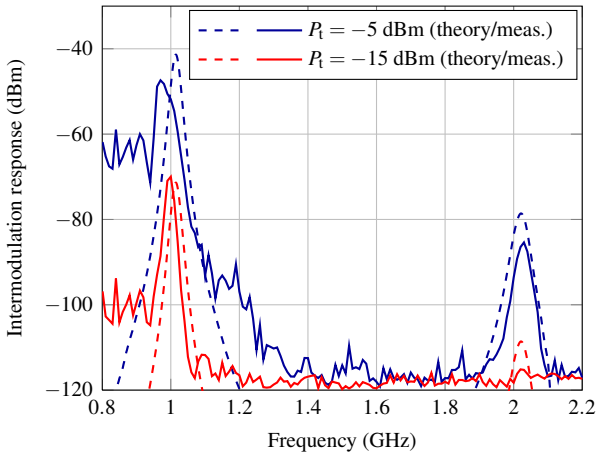

Fig. 4. Analytical (dashed) and measured (solid) response as a function of frequency with transmitter input power of −5 dBm (blue) and −15 dBm (red).

The signals are then amplified with two Milmega AS0822-8L linear power amplifiers, isolated with DITOM D3C0102S circulators and then connected through a power divider to an ETS-Lindgren 3164-08 quad-ridged horn antenna. The receiver consists of a similar antenna connected to an Anritsu MS2683A spectrum analyzer. The spectrum analyzer and signal generators are controlled via GPIB interface with a PC running LabVIEW virtual instrumentation.

The gain of the transmitter and receiver antennas (G_{ta}, G_{r}) is 8 dBi at 1 GHz and 9.5 dBi at 2 GHz. The gain of the transmitter chain (G_{tc}) is measured to be 29.6 dB at 1 GHz and 28.5 dB at 2 GHz. The losses in the receiver are measured to be 1.1 and 1.45 dB at 1 and 2 GHz, respectively.

The frequency offset is selected to be 300 kHz as the measurement equipment produces spurious signals that interfere with the measurement if the offset is smaller. The offset can be considered small compared to the operating frequency and bandwidth. The measured transponder is placed on a turntable 1.5 meters away from both the transmitter and the receiver. This ensures that the far-field conditions are met while still keeping the distance short to obtain a strong response. The selected distance also facilitated measurements in an anechoic chamber. The measurement setup is illustrated in Fig. 3.

B. Dynamic Range

The limitations of the small-signal model are investigated by measuring the response from 0.8 to 2.2 GHz in 10 MHz increments, adjusting the input power from 10 to 30 dBm. The measurement antennas are set to vertical polarization and they are placed along the omnidirectional plane of the transponder radiation pattern.

Fig. 4 illustrates the measured response at two different power levels. Analytical response is shown as well for comparison. The analytical model agrees well with the measurements, although the first resonance is at a lower frequency and the second resonance produces a smaller response. These can be assumed to be caused by slight differences between the simulated and manufactured transponder.

The measured response in Fig. 4 also contains distortion generated by the measurement equipment, appearing as increased noise floor at lower frequencies. The isolation of the circulators degrades at frequencies below 1 GHz, causing some of the transmitter-generated distortion to leak through. Despite being above the noise level, the interference is well below the transponder response and does not significantly affect the measurement result. At higher frequencies there is no detectable distortion and therefore attenuation before the receiver is not needed.

The limitations of the small-signal model can be seen occurring at the first resonance with high input power. The shape and amplitude of the resonance are altered because small-signal conditions are no longer valid. At power levels where the first resonance is still in accordance with the model, the second resonance is not visible. Conversely, when the second resonance is well above the noise level the model does not apply to the first resonance. This problem is notable for harmonic transponders that have two distinct frequency bands of interest but is absent in transponders operating only in one frequency band, such as conventional RFID tags. It should be noted that there is no need to measure both frequency bands at the same time. The two resonance frequencies could also have been measured separately, possibly adjusting the setup (e.g. distance, attenuation) to better suit the measured frequency band.

To further demonstrate the effect of input power, the power dependency at the frequencies of best matching (0.99 and 2.02 GHz) is shown in Fig. 5. The lower resonance frequency begins to diverge from the small-signal model when the power received by the tag increases above −10 dBm. On the other hand, with too small input power, the second resonance is obscured by noise. The small-signal conditions are satisfied at 2 GHz with all used power levels.

C. Gain and Radiation Pattern

The realized gain of the transponder is measured at the first resonance frequency of 0.99 GHz. Of the geometries discussed in Section III, we use the bistatic geometry as it is most suitable for our available equipment, and it should provide better dynamic range than the monostatic geometry. We also

This article has been accepted for publication in a future issue of this journal, but has not been fully edited. Content may change prior to final publication. Citation information: DOI 10.1109/TAP.2015.2414438, IEEE Transactions on Antennas and Propagation

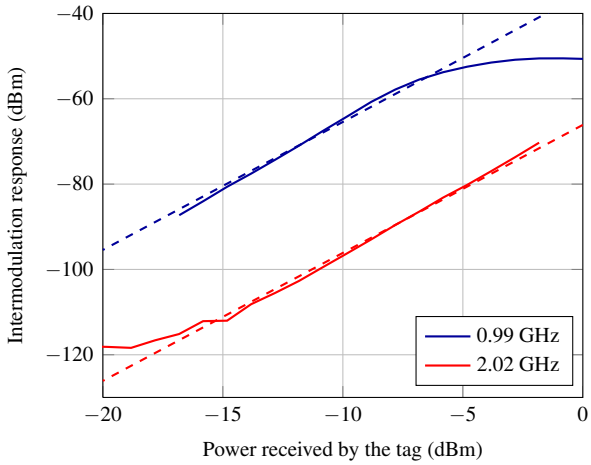

Fig. 5. Measured intermodulation response at 0.99 (blue) and 2.02 GHz (red) as a function of transmitted power (solid lines). The dashed lines represent the ideal behavior predicted by the model when the matching level is equal to that obtained from the measurements.

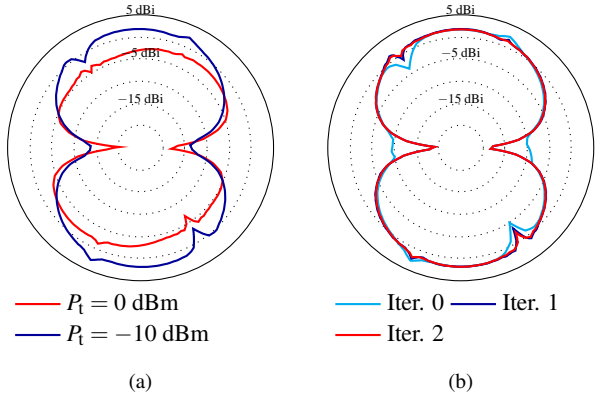

Fig. 6. Power dependency of the radiation pattern measurement. (a) The calculated gain with two different transmitter input power levels. (b) Calculated gain using the iterative power compensation.

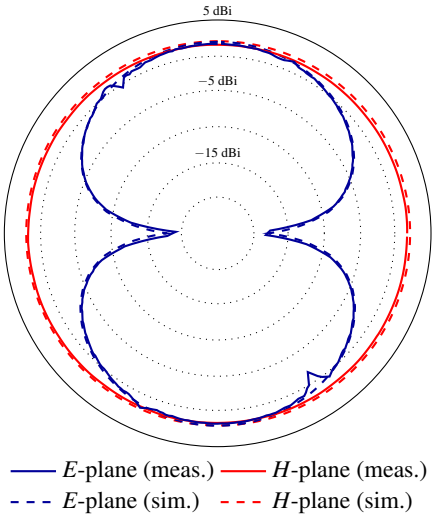

Fig. 7. Comparison of measured and simulated *E*-plane and *H*-plane radiation patterns at 0.99 GHz.

want to verify the equations derived for the bistatic geometry. Additionally, multistatic geometry has already been used in [20].

For the *E*-plane pattern measurement, the transmitter and receiver antennas are switched to horizontal polarization so that the tag can be rotated along the correct axis. The offset between the antennas is selected to be 60° and it is found that the measured distortion with this configuration is −115 dBm. The interference is transmitter-based, so it could not be reduced by attenuation and is therefore the limiting factor for the dynamic range. The offset is large enough to prevent both antennas facing the minima of the pattern simultaneously.

The pattern is measured with several different power levels as there is no constant input power at which the response would fit in the dynamic range. Either the minima are obscured by noise or the maxima are not within the constraints of the model. Fig. 6(a) illustrates this with the measured gain at two constant input powers, −10 and 0 dBm.

To increase the dynamic range, the input power is adjusted using (11). The initial input power is set to 15 dBm and the gain is calculated iteratively. Fig. 6(b) illustrates the effect of the iterations. The first iteration already improves the result significantly. Iterations after the second do not affect the results in a significant way.

There are slight errors in the pattern at angles offset by 60° from the minima. These are caused by the limited dynamic range of the measurement setup and they cannot be removed by power compensation. Due to the small SINR in the minima, the interference significantly affects the measured response, which causes the gain to be calculated erroneously. This could be avoided by having a measurement system with better dynamic range or by measuring the pattern with another antenna offset, such as by swapping the transmitter and receiver antennas.

The *H*-plane pattern of the transponder was measured as well. The antenna is omnidirectional in this plane so the measured pattern was almost constant. Therefore no power adjustments were needed.

Both measured gain patterns are then compared with patterns obtained from simulation software [23]. The results are shown in Fig. 7. The measurements agree well with the simulated patterns, with the exception of the errors caused by the low SINR.

D. Impedance Matching

The measured response is then used to calculate the impedance matching from (22). The input power is also adjusted using (11) to obtain small-signal operation for both resonance frequencies. The gain of the antenna is estimated from simulations. The results can be seen in Fig. 8. According to the results, the first resonance appears to have shifted slightly lower than what the simulations predicted. Additionally, the matching at the second resonance is somewhat worse than in the simulations. However, the magnitude calculation is rather sensitive to changes in the intermodulation response. Some differences are therefore expected. If E_{IM} of the circuit is not known, the absolute magnitude of the reflection coef-

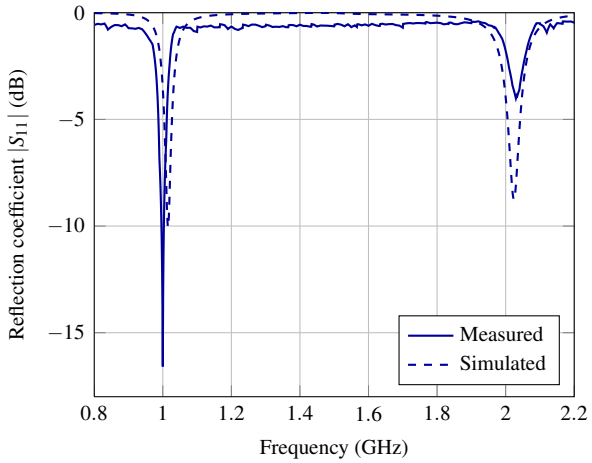

Fig. 8. Measured and simulated reflection coefficient $|S_{11}|$.

ficient cannot be obtained. The resonant frequencies and the bandwidth can be obtained from the results, even in this case.

VI. Conclusion

This paper has further analyzed the intermodulation measurement technique. We derived equations for the analytical intermodulation response of a transponder, using as an example a harmonic transponder with a Schottky diode. The derived response was then used to solve the antenna gain and impedance matching from the intermodulation response.

Three alternative measurement geometries were presented and their advantages and drawbacks were discussed. Limitations of the theoretical model were explained, as well as the dynamic range of the measurement technique.

The method was verified with measurements. The results showed good agreement between the theory and experiments, which suggests the validity of the analytical model and the measurement technique.

The technique is found to be well suited for characterizing harmonic transponders, for which no other reliable characterization method is known. The information about the impedance matching is especially useful for designing transponders with matching circuitry.

Future work could involve a more detailed analysis on the robustness and the error sources of the method, as well as further nonlinear analysis on different potentially usable circuits. One such circuit could be a specifically designed nonlinear load for characterizing other than transponder antennas.

VII. Acknowledgment

The authors would like to thank Dr. J. Ilvonen for useful discussions and on assistance in improving the measurement setup.

References

[1] J. Vogler, D. Maguire, and A. Steinhauer, "DINADE–a new interrogation, navigation and detection system," *Microwave Journal*, vol. 10, no. 4, pp. 2–6, Apr. 1967.

[2] J. Song, V. Viikari, N. Pesonen, I. Marttila, and H. Seppä, "Optimization of wireless sensors based on intermodulation communication," *IEEE Trans. Microw. Theory Tech.*, vol. 61, no. 9, pp. 3446–3452, Sep. 2013.

[3] V. Viikari, J. Song, and H. Seppä, "Passive wireless sensor platform utilizing a mechanical resonator," *IEEE Sensors J.*, vol. 13, no. 4, pp. 1180–1186, Apr. 2013.

[4] V. Viikari, H. Seppä, and D.-W. Kim, "Intermodulation read-out principle for passive wireless sensors," *IEEE Trans. Microw. Theory Tech.*, vol. 59, no. 4, pp. 1025–1031, Apr. 2011.

[5] V. Viikari, H. Seppä, T. Mattila, and A. Alastalo, "Wireless ferroelectric resonating sensor," *IEEE Trans. Ultrason., Ferroelectr., Freq. Control*, vol. 57, no. 4, pp. 785–791, Apr. 2010.

[6] V. Viikari and H. Seppä, "RFID MEMS sensor concept based on intermodulation distortion," *IEEE Sensors J.*, vol. 9, no. 12, pp. 1918–1923, Dec. 2009.

[7] V. Viikari, J. Chisum, and H. Seppä, "Wireless passive photo detector for insect tracking," *Microwave and Optical Technology Letters*, vol. 52, no. 10, pp. 2312–2315, Oct. 2010.

[8] K. Rasilainen, J. Ilvonen, and V. Viikari, "Antenna matching at harmonic operating frequencies to complex load impedance," *IEEE Antennas Wireless Propag. Lett.*, vol. 14, pp. 535–538, 2015.

[9] D. Mascanzoni and H. Wallin, "The harmonic radar: a new method of tracing insects in the field." *Ecological Entomology*, vol. 11, no. 4, pp. 387–390, Nov. 1986.

[10] J. Riley, A. Smith, D. Reynolds, A. Edwards, J. Osborne, I. Williams, N. Carreck, and G. Poppy, "Tracking bees with harmonic radar," *Nature*, vol. 379, no. 6560, pp. 29–30, Jan. 1996.

[11] B. Colpitts and G. Boiteau, "Harmonic radar transceiver design: miniature tags for insect tracking," *IEEE Trans. Antennas Propag.*, vol. 52, no. 11, pp. 2825–2832, Nov. 2004.

[12] RECCO Rescue System. Recco AB, Liding, Sweden. [Online]. Available: http://www.recco.com/about

[13] K. Rasilainen, J. Ilvonen, A. Lehtovuori, J.-M. Hannula, and V. Viikari, "On design and evaluation of harmonic transponders," *IEEE Trans. Antennas Propag.*, vol. 63, no. 1, pp. 15–23, Jan. 2015.

[14] R. F. Harrington, "Theory of loaded scatterers," *Proceedings of the Institution of Electrical Engineers*, vol. 111, no. 4, pp. 617–623, Apr. 1964.

[15] R. Garbacz, "Determination of antenna parameters by scattering cross-section measurements," *Proceedings of the Institution of Electrical Engineers*, vol. 111, no. 10, pp. 1679–1686, Oct. 1964.

[16] J. Appel-Hansen, "Accurate determination of gain and radiation patterns by radar cross-section measurements," *IEEE Trans. Antennas Propag.*, vol. 27, no. 5, pp. 640–646, Sep. 1979.

[17] J. T. Mayhan, A. Dion, and A. Simmons, "A technique for measuring antenna drive port impedance using backscatter data," *IEEE Trans. Antennas Propag.*, vol. 42, no. 4, pp. 526–533, Apr. 1994.

[18] P. Pursula, D. Sandstrom, and K. Jaakkola, "Backscattering-based measurement of reactive antenna input impedance," *IEEE Trans. Antennas Propag.*, vol. 56, no. 2, pp. 469–474, Feb. 2008.

[19] Voyantic Ltd. Espoo, Finland. [Online]. Available: http://www.voyantic.com

[20] M. Ritamäki, A. Ruhanen, V. Kukko, J. Miettinen, and L. H. Turner, "Contactless radiation pattern measurement method for UHF RFID transponders," *Electronics Letters*, vol. 41, no. 13, pp. 723–724, Jun. 2005.

[21] W. L. Stutzman and G. A. Thiele, *Antenna theory and design*, 3rd ed. Hoboken, NJ: John Wiley & Sons, 2012.

[22] Skyworks Solutions, Inc. Woburn, MA, USA. [Online]. Available: http://www.skyworksinc.com

[23] SEMCAD X, ver. 14.8. Aletsch, Schmid & Partner Engineering AG. Zurich, Switzerland. [Online]. Available: http://www.semcad.com

This article has been accepted for publication in a future issue of this journal, but has not been fully edited. Content may change prior to final publication. Citation information: DOI 10.1109/TAP.2015.2414438, IEEE Transactions on Antennas and Propagation

Jari-Matti Hannula was born in Luvia, Finland, in 1990. He received the B.Sc. (Tech.) degree in electrical engineering from Aalto University School of Electrical Engineering, Espoo, Finland, in 2014 and is currently pursuing the M.Sc. (Tech.) degree in electrical engineering at the same university.

He has worked as a Research Assistant and as a Teaching Assistant in the Department of Radio Science and Engineering, Aalto University School of Electrical Engineering, since 2013. From 2012 to 2013 he worked as a Teaching Assistant in the Department of Mathematics and Systems Analysis, Aalto University School of Science. His current research interests include wireless sensors, electrically small antennas, and antenna measurements.

Kimmo Rasilainen was born in Helsinki, Finland, in 1987. He received the B.Sc. (Tech.) and M.Sc. (Tech.) (with distinction) degrees in electrical engineering from Aalto University School of Electrical Engineering, Espoo, Finland, in 2012 and 2013, respectively, and is currently working toward the D.Sc. (Tech.) degree at the same university.

Since 2009, he has been with the Department of Radio Science and Engineering, Aalto University School of Electrical Engineering, first as a Research Assistant and currently as a Research Scientist. His research interests include handset antennas, user effect, bendable antenna structures and wireless sensor applications.

Ville Viikari (S'06–A'09–M'09–SM'10) was born in Espoo, Finland, in 1979. He received the Master of Science (Tech.), Licentiate of Science (Tech.) (with distinction), and Doctor of Science (Tech.) (with distinction) degrees in electrical engineering from the Helsinki University of Technology (TKK), Espoo, Finland, in 2004, 2006, and 2007, respectively.

He is currently an Assistant Professor with the Aalto University School of Electrical Engineering, Espoo, Finland. From 2001 to 2007, he was with the Radio Laboratory, TKK, where he studied antenna measurement techniques at submillimeter wavelengths and antenna pattern correction techniques. From 2007 to 2012, he was a Research Scientist and a Senior Scientist with the VTT Technical Research Centre, Espoo, Finland, where his research included wireless sensors, RFID, radar applications, MEMS, and microwave sensors. His current research interests include wireless sensors, RFID, and handset antennas

Dr. Viikari has served as the chair of the Technical Program Committee of the 6th ESA Workshop on Millimetre-Wave Technology and Applications and the 4th Global Symposium on Millimeter Waves (GSMM 2011), Espoo, Finland, 2011. He was the recipient of the Young Researcher Award of the Year 2014, presented by the Finnish Foundation for Technology Promotion, IEEE Sensors Council 2010 Early Career Gold Award, the 2008 Young Scientist Award of the URSI XXXI Finnish Convention on Radio Science, Espoo, Finland, and the Best Student Paper Award of the annual symposium of the Antenna Measurement Techniques Association, Newport, RI, USA (October 30–November 4, 2005).